Journal of Applied Electrochemistry **32**: 149–156, 2002.

Effect of temperature on stability of adsorbed inhibitors on steel in phosphoric acid solution

M.A. AMEER[1]*, E. KHAMIS[2] and G. AL-SENANI[3]
[1]*Chemistry Department, Faculty of Science, Cairo University, Egypt*
[2]*Chemistry Department, Faculty of Science, Alexandria University, Egypt*
[3]*College of Science, Chemistry Department, King Saud University, KSA*
*(*author for correspondence, e-mail: mameer_eg@yahoo.com)*

Received 31 May 2000; accepted in revised form 18 October 2001

Key words: adsorption isotherm, inhibitor, molecular structure, phosphoric acid, steel, temperature, thiosemicarbazide

Abstract

Rates of steel dissolution in 35% H_3PO_4/6% butanol (test solution) in the presence of thiosemicarbazide and seven of its derivatives were determined by spectrophotometry, weight loss and potentiodynamic and impedance techniques in the temperature range 303 to 333 K. At all temperatures, the corrosion rate decreased with increasing inhibitor concentration. Increasing temperature decreased the protection efficiency particularly at concentrations less than 2.5×10^{-4} M. At inhibitor concentrations above 2.5×10^{-4} M, increasing the temperature did not affect efficiency. Potentiodynamic polarization measurements indicated that the inhibitors have a strong effect on the corrosion behavior of the steel and behave as mixed type inhibitors. Thermodynamic functions obtained from this study indicate that the presence of the inhibitors increase the activation energy. The negative values of ΔG^* indicated spontaneous adsorption on the metal surface. A kinetic-thermodynamic model was found to describe the experimental well data at different temperatures.

1. Introduction

In previous studies [1, 2] thiosemicarbazide and its derivatives have been examined as corrosion inhibitors for mild steel in phosphoric acid solutions. When temperature is raised, corrosive processes are usually accelerated, especially in media in which evolution of hydrogen accompanies corrosion (e.g., during corrosion of steel in acids or of zinc in alkali). If oxygen takes part in a cathodic reaction during corrosion, the relationship between corrosion rate and temperature becomes more complicated owing to the lower solubility of oxygen at elevated temperature [3]. Calcott and Whetzel [4] showed, after examining extensive experimental data, which between 293 and 373 K the logarithm of corrosion rate is a linear function of temperature. An analogous relationship between rate constant and temperature in electrochemical reactions has been reported [5–7]. Machu [8] studied the influence of temperature on the action of dibenzyl sulphide, dibenzyl sulphoxide, aniline, gelatine, and other corrosion inhibitors for steel at 288, 320 and 348 K. He concluded that, in the presence of powerful inhibitors, the temperature coefficient as well as the corrosion rate is lowered. Sydberger and Nordin [9] studied the corrosion resistance of three stainless grades in wet process phosphoric acid of varying corrosivity. The polarization measurements showed that some salts such as sulfate and, in particular, fluoride markedly strengthens the depolarizing effect of chloride on the anodic dissolution in the active region. The effect of temperature on the inhibition of the acid corrosion of steel by benzaldehyde thiosemicarbazone using impedance measurements has also been studied [10]. An adsorption study has been reported on the corrosion inhibition of steel in H_3PO_4/organic solvent mixtures [11]. The organic solvents improved the corrosion resistance of steel to an extent depending on the concentration of the acid and the solvent, as well as on the different protic and stereochemistry properties of the alcohol. Thermodynamics of steel corrosion inhibition in phosphoric acid by ethylene trithiocarbonate [12] and in sulfuric acid containing cationic surfactants or organo-phosphorous derivatives was studied [13, 14]. Khamis [15] studied the corrosion of mild steel in sulfuric acid containing thiosemicarbazide derivatives over the temperature range 298 to 333 K using a.c. impedance spectroscopy. Results elucidated the effect of temperature and molecular structure on inhibition efficiency. The anodic dissolution process was under activation control for all the compounds investigated at different temperatures without affecting the mechanism of the dissolution process. Thermodynamic parameters

for adsorption of the compounds were calculated using the Temkin adsorption isotherm.

This paper describes a study of the electrochemical characteristics and kinetics of the corrosion process over the temperature range 303 to 333 K for six inhibitors in order to define the optimum temperature range for application.

2. Experimental details

A mild steel rod of chemical composition shown in Table 1 was used as working electrode. Specimens were mechanically polished with emery papers of different grades (320–600–1200). The rods were washed thoroughly with distilled water and dried with ethanol. The dissolved iron (Fe^{3+}) obtained from the natural immersion of steel samples in the 35% H_3PO_4/6% butanol was determined using spectrophotometric measurements at a wavelength (λ_{max}) of 535 nm. The dissolution of steel was characterized by a linear increase in the amount of dissolved Fe^{3+} with time. The inhibition efficiency of the compounds can be measured by evaluating the percentage protection efficiency, P, from the following relationship:

$$P = 100\left(1 - \frac{R_{inh}}{R_o}\right) \times 100 \quad (1)$$

where R_o and R_{inh} are the corrosion rates in the absence and the presence of a certain inhibitor concentration, respectively. The cleaned and polished steel sample was weighed before and after exposure to the acid solutions in the absence and presence of different inhibitor concentrations. The weight loss was determined in mg cm^{-2} min^{-1}. The efficiency of the inhibitors was calculated by evaluating the percentage reduction in weight loss, W, as follows:

$$W = 100\left(1 - \frac{w_{inh}}{w_o}\right) \times 100 \quad (2)$$

where, w_o and w_{inh} are the weight losses of steel in the absence and presence of inhibitor, respectively.

Potentiodynamic and impedance measurements were made using an ACM Instruments device (AutoTafel and AutoAC DSP). A Corning-type saturated calomel electrode (SCE) was used as reference electrode. The sweep rate used was 0.02 V min^{-1}. In impedance measurements, 10 points were measured for each decade of frequency ranging between 3 kHz–0.01 Hz. The capacitance of the double layer (C_{dl}) was calculated from [8]:

$$C_{dl} = \frac{1}{2\pi R_{ct} f} \quad (3)$$

where f is the frequency at the maximum height of the semicircle on the imaginary axis and R_{ct} is the charge transfer resistance. The protection efficiency, P_{ct}, of any particular compound at a specific temperature was calculated from the impedance data by applying the following relationship:

$$P_{ct} = 100\left(1 - \frac{R_{ct}^{-1}}{R_{cto}^{-1}}\right) \times 100 \quad (4)$$

where R_{cto}^{-1} and R_{ct}^{-1} are the reciprocals of the charge transfer resistance of steel in the absence and presence of inhibitor, respectively.

The studied compounds and their structural formulae are given in Table 2(a) and (b). Their preparation was described previously [1, 2].

3. Results and discussion

Figure 1 gives an example of the variation of the amount of dissolved iron ions (Fe^{3+}) as a function of time for mild steel immersed in 35% H_3PO_4/6% BuOH (test solution) in the absence and presence of different concentrations of CrTSCN at 313 K. At all temperatures, the rate of iron dissolution decreases with increasing CrTSCN concentration and the degree of inhibition depends on the concentration of the compound. The protection efficiency of CrTSCN at different temperatures is shown in Figure 2. The protection efficiency decreases with increasing temperature at concentrations less than 2.5×10^{-4} M as shown in Figure 3. This may be attributed to desorption of the inhibitor molecules from the metal surface at elevated temperature leading to a greater area of metal being exposed to the acid. However, at concentrations above 2.5×10^{-4} M, increasing the temperature does not affect the efficiency, that is, a strong film is chemisorbed on the surface of the metal in this temperature range. Figure 4(a) and (b) show potentiodynamic polarization curves of steel in the aerated test solution in the presence of 0.0001 M CrTSCN at different temperatures. The inhibitor has a strong effect on the corrosion behavior of the steel and the inhibitor behaves as a mixed type. This effect of the inhibitor appears to be dependent on the temperature of the medium. According to Epelboin and co-workers [16], a.c. impedance measurements for metal dissolution in acid media in the presence of inhibitors can be interpreted in terms of the charge transfer resistance, R_{ct}, which is defined as the limiting zero frequency value of the real part of the complex impedance. Moreover, it was reported that R_{ct} was more intimately correlated to the corrosion rate than the

Table 1. Chemical composition of the steel specimens

C	Si	Mn	P	S	Cu	Cr	Mo	Ni	Sn	V
0.31	0.21	0.81	0.014	0.017	0.06	0.02	0.01	0.02	0.0	0.002

Table 2. (a) Investigated compounds of first group

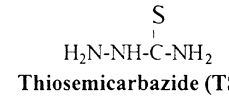

Thiosemicarbazide (TSC)

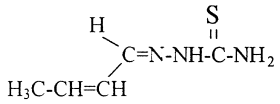

Crotonaldehyde thiosemicarbazone (CrTSCN)

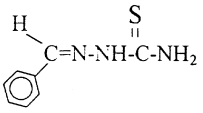

Benzaldehyde thiosemicarbazone (BTSCN)

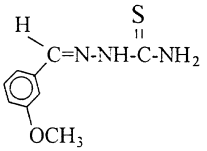

Methoxybenzalaldehyde thiosemicarbazone (MBTSCN)

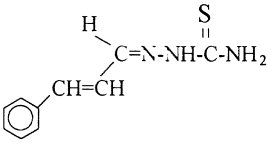

Cinnamaldehyde thiosemicarbazone (CTSCN)

(b) Investigated compounds of the second group

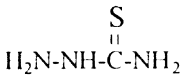

Thiosemicarbazide (TSC)

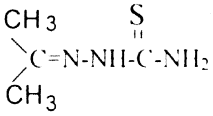

Acetone thiosemicarbazone (ATSCN)

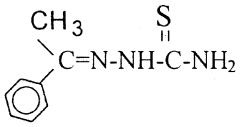

3-Acetophenone thiosemicarbazone (AphTSCN)

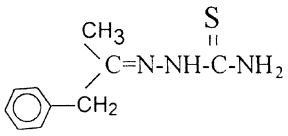

Phenylacetone thiosemicarbazone (PATSCN)

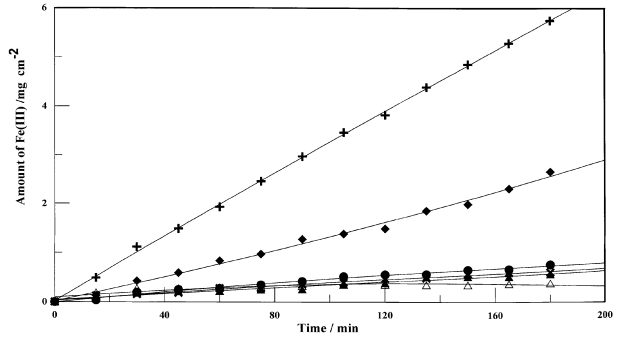

Fig. 1. Amount of Fe(III) against time curves for steel for different concentration of CrTSCN at 313 K. Key: (+) test solution, (◆) 1.0×10^{-5}, (●) 5.0×10^{-5}, (▲) 7.5×10^{-5}, (×) 1.0×10^{-4} and (△) 1.0×10^{-3} M.

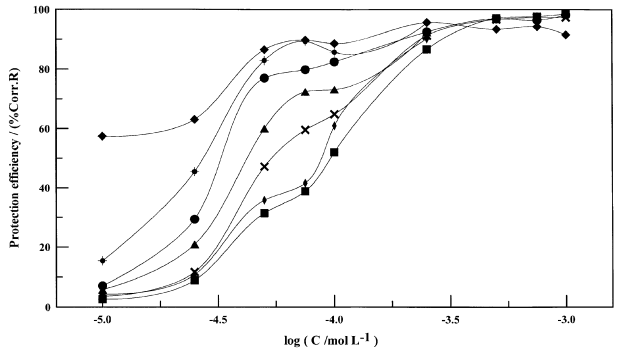

Fig. 2. Relationship between the inhibition efficiency of CrTSCN with logarithmic concentration at different temperatures. Key: (◆) 303, (✦) 308, (●) 313, (▲) 318, (×) 323, (♦) 328 and (■) 333 K.

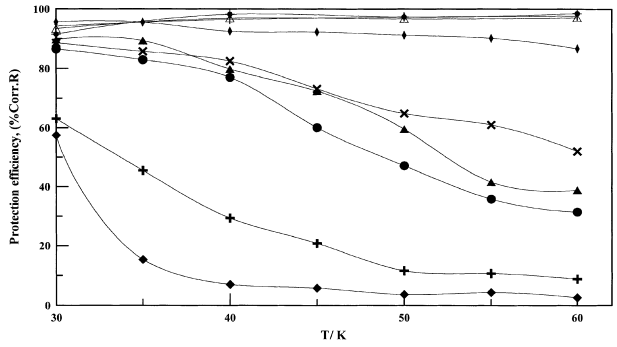

Fig. 3. Relationship between the inhibition efficiency of CrTSCN and temperature at different concentrations. Key: (◆) 1.0×10^{-5}, (+) 2.5×10^{-5}, (●) 5.0×10^{-5}, (▲) 7.5×10^{-5}, (×) 1.0×10^{-4}, (♦) 2.5×10^{-4}, (✦) 5.0×10^{-4}, (↑) 7.5×10^{-4} and (△) 1.0×10^{-3} M.

polarization resistance, R_p. Electrochemical theory shows that (R_{ct}^{-1}) is proportional to the corrosion rate, and is analogous to the use of polarization resistance in the Stern–Geary equation:

$$I_{corr} = \frac{\beta_a \times \beta_c}{2.3(\beta_a + \beta_c)} \times \frac{1}{R_{ct}} \tag{5}$$

$$I_{corr} = \frac{\text{constant}}{R_{ct}} \tag{6}$$

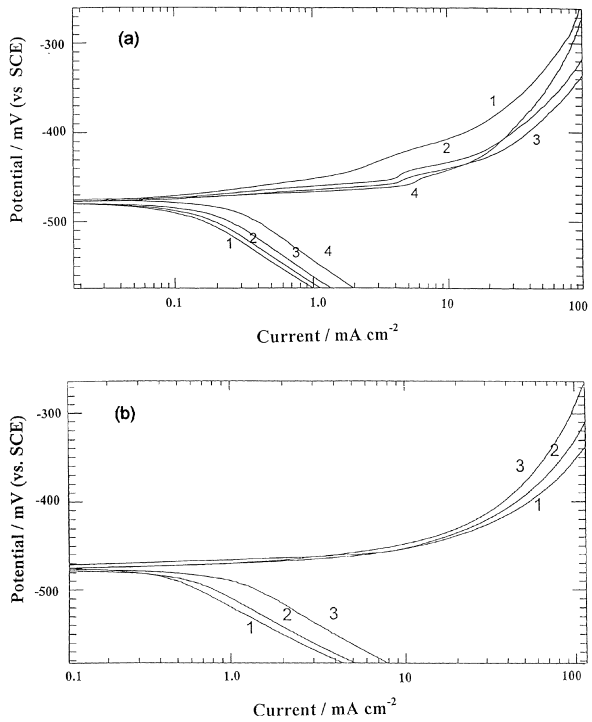

Fig. 4. (a) Polarization curves of mild steel in the presence of 0.0001 M CrTSCN at 303, 308, 313 and 318 K. Key: (1) 303, (2) 308, (3) 313 and (4) 318 K. (b) Polarization curves of mild steel in the presence of 0.0001M CrTSCN at 323, 328 and 333 K. Key: (1) 323, (2) 328 and (3) 333 K.

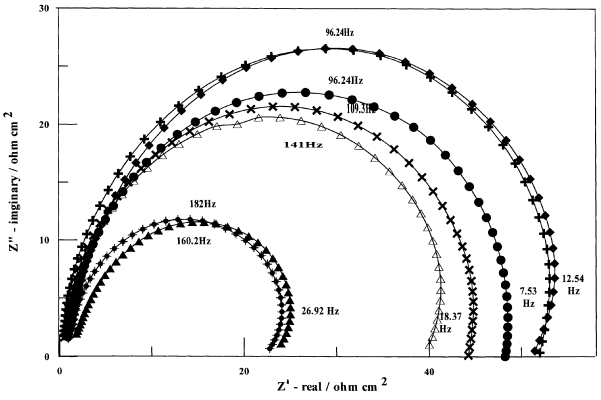

Fig. 5. Nyquist diagrams of mild steel for 0.0001 M CrTSCN at different temperatures. Key: (+) 303, (◆) 308, (●) 313, (×) 318, (△) 323 (✦) 328 and (▲) 333 K.

Figure 5 shows Nyquist diagrams for mild steel at the rest potential in the aerated test solution containing 0.0001 M CrTSCN at different temperatures. The complex impedance plots have the appearance of a semicircle for all solutions examined. A characteristic feature is the absence of a diffusive contribution at low frequencies. This indicates that the charge transfer controls the dissolution mechanism of steel across the phase boundary in the presence and absence of inhibitor. Moreover, the presence of inhibitor does not alter the dissolution mechanism. The results also indicate that increase in temperature leads to a decrease in the charge transfer resistance value, R_{ct}, hence increasing the corrosion rate.

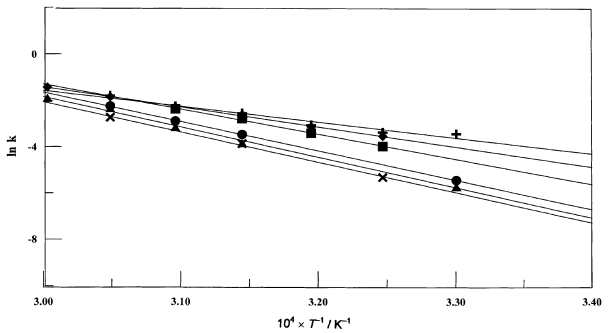

Fig. 6. Arrhenius plot of the corrosion rate of steel in the absence and presence of different concentration of CrTSCN at different temperature. Key: (+) test solution, (◆) 1.0×10^{-5}, (■) 2.5×10^{-5}, (●) 5.0×10^{-5}, (▲) 7.5×10^{-5} and (×) 1.0×10^{-4} M.

The activation parameters such as apparent activation energy (E_a^*), the enthalpy change of activation (ΔH^*), and the entropy change of activation (ΔS^*), are obtained from an Arrhenius-type plot (Equation 7) and Eyring transition-state (Equation 8):

$$\ln k = \frac{-E_a^*}{RT} + A \tag{7}$$

$$\ln\left(\frac{k}{T}\right) = -\left(\frac{\Delta H^*}{RT}\right) + \ln\left(\frac{R}{N_A h}\right) + \left(\frac{\Delta S^*}{R}\right) \tag{8}$$

where k is the corrosion rate in the absence and presence of inhibitors, R is the universal gas constant, A is the frequency factor, N_A is Avogadro's number and h is Planck's constant. Plots of ln k against $1/T$ and In (k/T) against $1/T$ give straight lines with slopes of $-E_a^*/R$ and $-\Delta H^*/R$, respectively. The intercepts are A and $[\ln(R/N_A h) + \Delta S^*/R]$ for Arrhenius and Eyring transition-state equations, respectively. Figure 6, shows least-squares plots for the ln k against $1/T$ data, the values of the activation energy obtained from the slopes of the lines at different temperatures are given in Table 3. Figure 7 shows least-squares plots for $\ln(k/T)$ against $1/T$ for different concentrations of CrTSCN. The plots are also linear. The calculated values of ΔH^* and ΔS^* obtained from these plots are tabulated in Table 3. Due to the presence of CrTSCN in the medium, the values of E_a^* and ΔH^* are lowest in the uninhibited solution. Moreover, increase in inhibitor concentration leads to

Table 3. Activation parameters of the dissolution of steel in 35% H_3PO_4/6% BuOH in the absence and presence of different concentrations of CrTSCN

10^4 C /M	E_a^* /kJ mol^{-1}	ΔH^* /kJ mol^{-1}	ΔS^* /J mol^{-1} K^{-1}
0.00	56.9	54.3	−92.9
0.10	72.0	69.4	−49.4
0.25	90.1	87.5	5.9
0.50	105.3	102.7	48.5
0.75	108.8	106.2	57.4
1.00	108.6	105.9	54.8

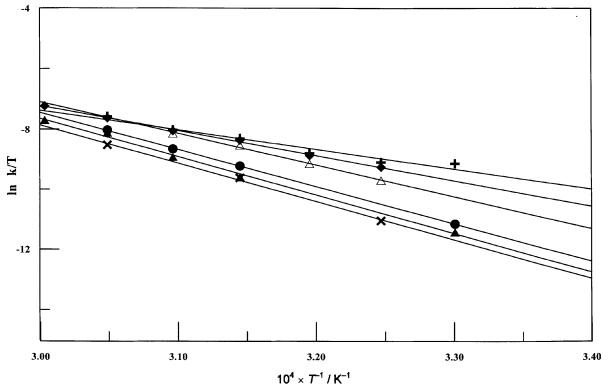

Fig. 7. Eyring plot of the corrosion rate of steel in the absence and presence of different concentration of CrTSCN at different temperature. Key: (+) test solution, (◆) 1.0×10^{-5}, (△) 2.5×10^{-5}, (●) 5.0×10^{-5}, (▲) 7.5×10^{-5} and (×) 1.0×10^{-4} M.

an increase in the value of E_a^*, indicating strong adsorption of the inhibitor molecules at the metal surface. The table also shows that the presence of the inhibitor produces higher values for ΔH^* than those obtained for the uninhibited solution. This indicates higher protection efficiency. This may be attributed to the presence of an energy barrier for the reaction, that is, the process of adsorption leads to a rise in the enthalpy of the corrosion process. The table illustrates that ΔS^* has negative values for the test solution and for the lowest concentration of the inhibitor (10^{-5} M CrTSCN). Thereafter ΔS^* values turned positive and increased steadily. Grigoryev [17, 18] and Antropov [19] have discussed this phenomenon. As in the free acid solutions, the transition state of the rate determining recombination step represents a more orderly arrangement relative to the initial state. Hence, a negative value for the entropy of activation is obtained. In the presence of the inhibitors, however, the rate-determining step is the discharge of hydrogen ions to form adsorbed hydrogen atoms. Since the surface is covered with the inhibitor molecules, this will retard the discharge of hydrogen ions at the metal surface causing the system to pass from a more orderly to a random arrangement, and hence positive entropy of activation is observed.

3.1. *Kinetic-thermodynamic model and adsorption isotherms analyses*

The data obtained from d.c. measurements have been fitted to the kinetic thermodynamic model in terms of the active site occupancy parameter, y, and the binding constant of the inhibitor with the metallic surface, k, as will be discussed later. The results are compared with fits executed from application of Langmuir, Frumkin and Flory–Huggins adsorption isotherms.

The results of data fitting for CrTSCN to Langmuir isotherm (Equation 9), Frumkin isotherm (Equation 10) and Flory–Huggins isotherm (Equation 11) indicate that the data do not fit any of them with a correlation coefficient less than 0.8:

$$\frac{\theta}{1-\theta} = kC \tag{9}$$

$$\left[\frac{\theta}{1-\theta}\right] \exp[-2a\theta] = kC \tag{10}$$

$$\frac{\theta}{x(1-\theta)^x} = kC \tag{11}$$

where θ is the surface coverage, C is the inhibitor concentration and a is the molecular interaction parameter depending on the molecular interactions in the adsorption layer and on the degree of surface heterogeneity. In the limit when $x = 1$ and $a = 0$, the Frumkin isotherm reduces to the Langmuir isotherm where x is the size ratio and is simply the number of water molecules replaced by one organic adsorbate molecule according to the following reaction:

$$(\text{inh})_{\text{aq}} + x\text{H}_2\text{O}_{\text{Sur}} \rightarrow \text{inh}_{\text{Sur}} + x(\text{H}_2\text{O})_{\text{aq}} \tag{12}$$

where $(\text{inh})_{\text{aq}}$ is the inhibitor molecules in the aqueous phase and $(\text{H}_2\text{O})_{\text{Sur}}$ is the water molecules adsorbed on the electrode surface. Khamis et al. [20] reported that the adsorption isotherms are generally of the following form:

$$f(\theta, x) \exp(-a\theta) = kC \tag{13}$$

where $f(\theta, x)$ is the configuration factor that depends essentially on the physical model and assumptions underlying the derivation of the isotherm surface. All expressions for adsorption isotherms include the equilibrium constant of the adsorption process, K, which is related to the standard free energy of adsorption, $\Delta G^\circ_{\text{ads}}$, by

$$K = \frac{1}{55.5} \exp \frac{-\Delta G^\circ_{\text{ads}}}{RT} \tag{14}$$

The curve fitting of the obtained data using CrTSCN to kinetic-thermodynamic model (Equations 15 and 16) [21, 22] is given in Figure 8:

$$\log\left(\frac{\theta}{1-\theta}\right) = \log K' + y \log C \tag{15}$$

$$K = K'^{(1/y)} \tag{16}$$

Good straight lines fit are obtained for different temperatures. The slope of the lines represents y, the number of inhibitor molecules occupying a single active site at each temperature. The intercept is $\log K'$ and $(1/y)$ gives the number of active sites occupied by a single inhibitor molecule. Table 4 gives the adsorption parameters such as number of active sites, binding constants and free energy of adsorption obtained from the kinetic-thermodynamic model using CrTSCN at different temperatures. The data confirm desorption of

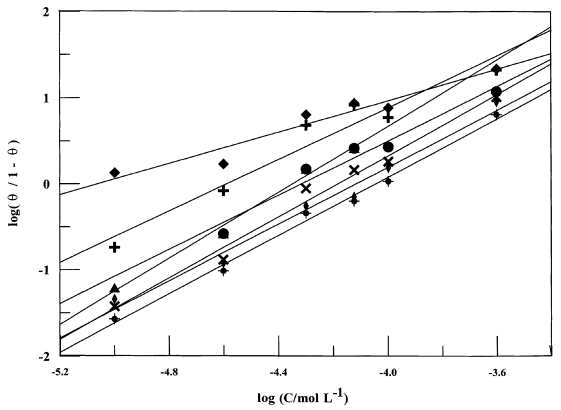

Fig. 8. Curve-fitting of the corrosion data of steel in different CrTSCN concentrations to the kinetic-thermodynamic model at different temperatures. Key: (+) 303, (+) 308, (●) 313, (▲) 318, (×) 323 and (◆) 328 and (⧫) 323 K.

Table 4. Binding constant, number of active sites values and free energy change obtained from the kinetic-thermodynamic model for 0.0001 M CrTSCN at different temperatures

Temp. /K	Kinetic-thermodynamic model		
	$1/y$	K	ΔG°_{ads}/kJ mol^{-1}
303	1.100	115 900	−39.51
308	0.509	40 492	−37.47
313	0.633	20 875	−36.35
318	0.520	22 493	−37.13
323	0.560	15 369	−36.70
328	0.603	13 195	−36.84
333	0.556	11 826	−37.10

the inhibitor molecules from the metal surface at elevated temperatures. The equilibrium constant of adsorption decreased with increasing the solution temperature from 115 900 at 303 K to 11 826 at 333 K. These results verify the data obtained from the percentage inhibition versus the logarithm of the inhibitor concentration at different temperatures which was discussed in the previous section. The large values of standard free energy of adsorption, ΔG°_{ads}, lie above 36 kJ mol^{-1} and have a negative sign indicating that the reaction proceeds spontaneously and is accompanied by an efficient adsorption. Additional information revealed from the kinetic-thermodynamic model suggests that the number of centers of the active sites decrease with increasing temperature. For CrTSCN at temperatures higher than 303 K, the calculated number of active sites is about half, which means that the inhibitor molecule will occupy more than one active site.

3.2. *Molecular structure effect*

The compounds employed in this study are divided into two main groups according to their chemical structure as shown in Tables 2(a) and (b).

It is necessary to reach a particular concentration value (threshold concentration) before the additive

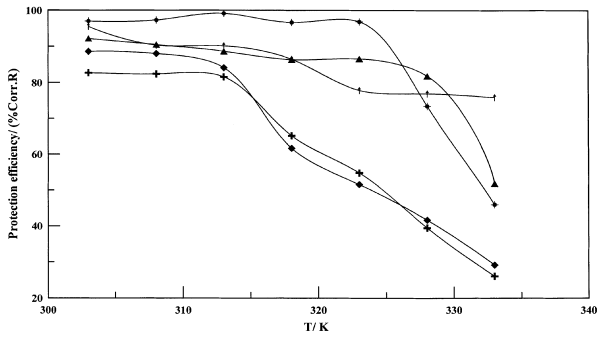

Fig. 9. Variation of protection efficiency with temperature for 0.0001 M of the first group compounds. Key: (+) test solution, (◆) CrTSCN, (▲) BTSCN, (↑) MBTSCN and (⧫) CTSCN.

begins to exert an inhibiting effect on the corrosion process [23]. Above this threshold concentration, the inhibiting efficiency first increases rapidly with concentration, then it increases slowly tending asymptotically to a limiting value. As reported earlier [1, 2], the inhibition reaches a maximum value before leveling off for the compounds of the first and second groups at a concentration of 0.0001 M, which is used in this study as a critical concentration. The variation of protection efficiency obtained from spectrophotometry measurements for 0.0001 M of the inhibitors of the first group at different temperatures are represented in Figure 9. Thiosemicarbazides could be physically adsorbed on the surface of the metal through its thio group forming a bond between their polar atoms and the metal. In other words, thiosemicarbazides are adsorbed by donating a pair of unshared electrons to an unoccupied orbital of a metal. Since the inhibitors and the metal are equivalent to Lewis bases and Lewis acids, respectively, the inhibition effects of the inhibitors are expected to be closely related to the hard and soft acids and bases (HSAB) principle [24]. The adsorption will leave the rest of the molecule (tail) to interact through van der Waal forces forming a hood covering the adsorbed functional group. This mode of adsorption resists the diffusion of hydrogen from the bulk solution to the metal surface and thus retards the dissolution of steel. The inhibition efficiency of mild steel corrosion in phosphoric acid by the compounds of the first group has the following order:

$$\text{CTSCN} > \text{MBTSCN} > \text{BTSCN} > \text{CrTSCN} > \text{TSC}$$

The difference in the efficiency may be attributed to the molecular structure effect. This behaviour is due to the rigidity of the π-delocalized system of CrTSCN, BTSCN, MBTSCN, and CTSCN compared to the saturated TSC molecule that permits free rotation, thus decreasing the possibility of its attachment to the metallic surface. The presence of an alkyl radical adjacent to the thio group also increases the electron density on the thio group and leads to an easier electron transfer from the functional group (C=S) to the metal,

producing greater coordinate bonding and hence greater adsorption and inhibition efficiency. It is clear that the substitution of the terminal hydrogen in the hydrazino-group of the thiosemicarbazide molecule has a dramatic influence on increasing the efficiency. Evidently this behaviour can be attributed to the increase in π-electron density on the ligating sulphur atom as a result of the inclusion of an alkyl group that possesses a high electron density compared to hydrogen. Thus, BTSCN shows a slight increase in the protection efficiency as compared to CrTSCN. This behaviour can be explained on the basis of the presence of the phenyl group attached to the azomethine increasing its electron density rather than the propene radical of BTSCN. Bringing together the methoxy group to the phenyl ring in the meta position will enhance the electron density on the centre of adsorption to a greater extent in the case of MBTSCN than in BTSCN. Finally, CTSCN may be considered as the best in this series since it possesses a number of double bonds.

The influence of the change in molecular structure of the second group compounds on the inhibition efficiency at different temperatures has been detected at a critical concentration of 0.0001 M over the temperature range 303–333 K. Figure 10 represents the variation of percentage protection efficiency as a function of temperature for 0.0001 M TSC, ATSCN, AphTSCN and PATSCN. The inhibition efficiency decreases as temperature increases and the inhibitors can be arranged according to their inhibition efficiency according to the following order:

PATSCN > AphTSCN > ATSCN > TSC

This arrangement may be attributed to the increase of both the number of double bonds and the number of carbon atoms that enhance the protection efficiency markedly. Thus, the highest protection efficiency obtained for PATSCN is due to the inclusion of the benzyl group containing a heterocyclic moiety carrying a high electron density compared to hydrogen leading to increase of the delocalized π-electron density of the center of adsorption.

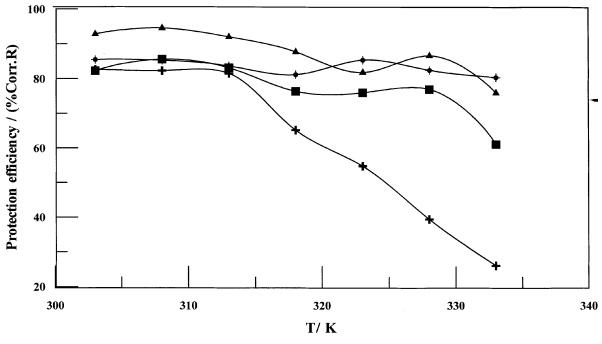

Fig. 10. Arrhenius plot of the corrosion rate of steel in the absence and presence of 0.0001 M of the second group compounds. Key: (+) test solution, (■) ATSCN, (♦) AphTSCN and (▲) PATSCN.

Table 5. Activation parameters of the dissolution of steel in 35% H_3PO_4/6% BuOH in the absence and presence of 0.0001 M of TSC, CrTSCN, BTSCN, MBTSCN, CTSCN, ATSCN, AphTSCN and PATSCN

Compound	E_a^*/kJ mol^{-1}	ΔH^*/kJ mol^{-1}	ΔS^*/kJ mol^{-1}
Test solution	43.82	41.18	−138.40
TSC	83.92	81.30	−21.85
CrTSCN	102.31	99.67	35.35
BTSCN	107.28	104.60	43.47
MBTSCN	140.91	138.24	148.54
CTSCN	168.14	165.47	225.80
ATSCN	87.39	84.71	−15.01
AphTSCN	96.16	93.43	6.36
PATSCN	99.31	78.43	17.66

Arrhenius and Eyring plots for 0.0001 M of each of the first and the second groups in the acid medium were used to obtain the activation parameters given in Table 5. The values of activation energy and enthalpy of activation in the presence of 0.0001 M of the above-mentioned inhibitors were higher than those of the uninhibited solution. In addition, the entropy of activation changes sign from negative to positive due to addition of efficient inhibitors and the positive value increases as the efficiency increases. Since the rate-determining step is the discharge of hydrogen ions to form adsorbed hydrogen atoms on the steel surface, the presence of efficient molecules will almost completely cover the surface leading to prevention of discharge process.

4. Conclusions

The results obtained from potentiodynamic polarization indicate that compounds of the first and second groups are mixed-type inhibitors. The a.c. measurements show that the charge-transfer resistance increases as the inhibitor concentration increases. The data obtained from a.c. impedance measurements at different temperatures in the presence of the different inhibitors indicate that the corrosion process is still under charge-transfer control, and R_{ct} decreases with increasing temperature. The kinetic-thermodynamic model and Flory–Huggins adsorption isotherm describe the experimental data well. The number of active sites, binding constant and change of free energy were computed for the inhibitors used. Thermodynamic values obtained, E_a^*, ΔH^*, ΔS^* and ΔG^*, indicate that the presence of the inhibitors increase the activation energy, and the negative values of ΔG^* indicate the spontaneous adsorption of the inhibitors on the mild steel surface.

Acknowledgement

This work was supported by a grant from King Abdul-Aziz City for Science and Technology (KACST), Riyadh, Saudi Arabia.

References

1. E. Khamis, M. Ameer, N. AlAndis and G. Al-Senani, *Corrosion* **56** (2000) 127.
2. M. Ameer, E. Khamis and G. Al-Senani, *Adsorption Sci. & Technol.* **18** (2000) 2.
3. I.N. Putilova, S.A. Balezin and V.P. Barannik, 'Metallic Corrosion Inhibitors' (Pergamon Press, New York, 1960), p. 55.
4. W.S. Calcott and J.C. Whetzel, *Trans. Am. Inst. Chem. Eng.* **35** (1923) 1.
5. S.V. Gorbachev, *Zh. Fiz. Khim* **24** (1950) 888.
6. S.V. Gorbachev and R.M. Vasenin, *Zh. Fiz. Khim. (Russia)* **28** (1954) 135.
7. A.V. Izmailov, *Zh. Fiz. Khim. (Russia)* **30** (1956) 2813.
8. W. Machu, *Korros. u. Metalls.* **14** (1938) 324.
9. T. Sydberger and S. Nordin, *Corrosion* **34** (1978) 16.
10. B. Abd El-Nabey, E. Khamis, G. Thompson and J. Dawson. *Surf. Coat. Technol.* **28** (1986) 83.
11. E. Khamis and A. Hosny, *Adsorption Sci. & Technol.* **12** (1995) 67.
12. E. Khamis, A. Hosny and S. El-Hadary, *Afinidad* **456** (1995) 95.
13. H.A. Al-Lohedan, E. Khamis and Z.A. Issa, *Adsorption Sci. & Technol.* **13** (1996) 137.
14. E. Khamis, M.N. Moussa, E.S.H. El-Ashry and A.K. Ibrahim, *Adsorption Sci. & Technol.* **13** (1996) 197.
15. E. Khamis, *Corrosion* **46** (1990) 476.
16. I. Epelboin, M. Keddam and H. Takenouti, *J. Appl. Electrochem.* **2** (1972) 71.
17. V.P. Grigorev and V.U. Eklik, *Prot. Met.* **4** (1968) 517.
18. V.P. Grigorev and O.A. Osipov, 3rd European Symposium on 'Corrosion Inhibitors', Ferrara, Italy (1970), p. 473.
19. L.A. Antropov and Y.A. Suvgira, *Prot. Met.* **3** (1967) 597.
20. E. Khamis, F. Bellucci, R. Latanision and E. El-Ashry, *Corrosion* **47** (1991) 677.
21. A. El-Awady, B. AbdEl-Nabey and Aziz, *J. Electrochem. Soc.* **135** (1992) 2149.
22. A. El-Awady, B. Abd El-Nabey and G. Aziz, M. Khalifa and H. Al-Ghamdy, *Int. J. Chem.* **1** (1991) 169.
23. A. Frignani, G. Trabanelli, F. Zicchi and M. Zucchini, Proc. 5th European Symposium on 'Corrosion Inhibitors', Ferrara, Italy (1980) 1185.
24. I. Epelboin, M. Keddam and H. Takenouti, *J. Appl. Electrochem.* **2** (1972) 71.